Study on the Dynamic Characteristics of an Integrated Coal Gasification Fuel Cell Combined Cycle

Shin'ya Obara

Power Engineering Lab., Dep. of Electrical and Electronic Engineering, Kitami Institute of Technology

Koen-cho 165, Kitami, Hokkaido 090-8507, Japan

obara@mail.kitami-it.ac.jp

phone/FAX +81-157-26-9262

Jorge Morel

Power Engineering Lab., Dep. of Electrical and Electronic Engineering, Kitami Institute of Technology

Masaki Okada

Dep. of Mechanical Systems Engineering, National Institute of Technology, Asahikawa College, Shyunkodai 2-2-1-6, Asahikaw, Hokkaido 071-8142, Japan

Kazuma Kobayashi

Technology Innovation Center, National Institute of Technology, Asahikawa College, Shyunkodai 2-2-1-6, Asahikaw, Hokkaido 071-8142, Japan

Abstract

In this study, a dynamic analysis model for integrated gasification fuel cell (IGFC) power generation was developed and the dynamic characteristics of electric power output by the

system were investigated. Using the proposed analytical model, the study addressed the frequency deviation of electric power output, the inertia system of gas and steam turbines, the air–fuel ratio of the solid oxide fuel cell (SOFC), and load patterns. Moreover, using the model, an example of an electric power load pattern in Japan was examined. Because the supply and demand difference in electric power can be monitored as frequency deviation in a power network, the frequency of each power generator was analyzed. Consequently, the output of IGFC gas and steam turbines could not be controlled in the target range. Therefore, it was necessary to stabilize the quantity of exhaust heat by improving the heat transfer speed of the SOFC.

Keywords: Integrated Coal Gasification Fuel Cell, Combined Cycle, Dynamic Characteristics, Solid Oxide Fuel Cell, Numerical Analysis

1. Introduction

Coal has many recoverable reserves and continues to be an important source of energy in the world. Because coal generates more CO_2 emissions than other energy sources, it is desirable to increase the power generation efficiency of coal-fired power plants. The integrated gasification fuel cell (IGFC) consists of an air separator, coal gasification furnace, solid oxide fuel cell (SOFC), gas turbine (G/T), and steam turbine (S/T). The IGFC is generated using synthesized H_2 gas produced by the coal gasifier. A power generation efficiency of 50% or more is realized using the combined cycle SOFC, G/T, and S/T [1-5]. The design of fundamental system [5-10], capture of CO_2 [11, 12], cleanup of synthesis gas

[13-15], exergy analysis, and economical efficiency [1-3, 16-20] are reported in a recent study on IGFC. Furthermore, case studies of SOFC power generation system using gasification of biomass [21-27], the SOFC organic Rankine cycle power system [28], the SOFC Stirling engine power system [29-32], the application to a distributed power supply [33], and study of a plasma gasifier fuel cell [34] have been conducted. Coal gasifiers in fixed bed, fluidized bed, entrained flow, and molten bath have also been developed [35]. Several types of coal gasifiers including a shell gasifier have been modeled. The dynamic characteristics of the IGFC are an important parameter required for the design of an electric power system. However, investigations of the dynamic characteristics of the IGFC have rarely been conducted, and the examination of output distribution and output stability using parallel operation of the IGFC and other power sources is not progressing. Although a large-scale IGFC is assumed to be the base supply of an electric power system, its use as a distributed power supply at a small or medium scale is analyzed in this study. Therefore, this study focuses on the dynamic characteristics of the IGFC using a numerical analysis model. The model developed in this study consists of the transient response characteristics of the SOFC triple combined cycle accompanied by the external reformer of natural gas developed in a previous study [36], and the analytical models of the integrated gasification combined cycle. By applying the analytic model to the IGFC with the full force power of 100 MW, the dynamic characteristics of the system are investigated using the MATLAB/Simulink R 2015a. Research findings have reported that the combined cycle by an SOFC and a gas turbine without a steam turbine is fine [37]. However, the

development of the SOFC triple combined cycle continues in Japan [38]. Therefore, the triple combined cycle comprising an SOFC, a gas turbine, and a steam turbine is examined.

2. System Configuration

2.1 Air Separation Unit (ASU)

The design of an air separation unit (ASU) has been presented in a previous study [39, 40]. The system configuration of the proposed IGFC and the flow of fluid and energy are shown in Fig. 1. The ASU for the proposed system assumes an internal compression type wherein raw material air is supplied by the air compressor $CP_{asu,air}$. Air is cooled using a precooler (cooling tower) and moisture and carbon dioxide are removed in the absorber. The ASU produces high purity nitrogen and 95% pure oxygen used by the coal gasifier. This oxygen is then used as the raw material for coal gasification. Pure nitrogen is used for parsing and conveyance during coal pressurization.

2.2 Coal Gasifier

This study assumed the introduction of an entrained flow coal gasifier to which the fine ground coal is supplied. Because the oxygen produced by the ASU is also supplied to the gasifier, the fine ground coal instantly reacts under partial oxidation. The high temperature synthesized gas of 1300 to 1600 $^{\circ}C$ generated by the gasifier is used for generating steam supplied to the S/T. The processing of the removal of toxic substances is performed in the gasifier unit. For example, particulates are removed by the particulate

scrubber at the gasifying furnace exit. The cleanup of gases does not have a large influence on the dynamic characteristics of the system.

2.3 SOFC Triple Combined Cycle

The raw synthesized gas produced by the gasifier is supplied to the anode in the SOFC and oxygen (air) is supplied to the cathode using an air compressor. The exhaust gas from both electrodes and air from the air compressor are burned and high temperature exhaust gas is supplied to the G/T. The exhaust heat from the G/T is supplied to a heat recovery steam generator and steam is supplied to the S/T. Although the electric power from the system is supplied to the demand side through a transmission network, the magnitude of the supply and demand balance appears as the frequency deviation. Accordingly, if there is more supply than the quantity demanded, the electric power frequency will increase from the rated value. If the amount of supply is less than the quantity demanded, the frequency will decrease from the rated value. Therefore, it is necessary to adjust the production of the IGFC so that the frequency deviation of electric power is allowed to decrease.

3. Modeling of the System

3.1 ASU

3.1.1 Mass Balance and Heat Balance

Air entering the compressor $CP_{asu,air}$ is separated into oxygen, nitrogen, and other gases. The air is compressed to about 0.5 MPa and as a result its temperature increases to about

80 °C. The heated air is then cooled to about 10 °C using a flush cooling tower. In addition, adsorption equipment removes moisture and carbon dioxide, and material gas is cooled to about −200 °C. Each ingredient is then separated in the cold box using the difference of the boiling point of each ingredient of the raw material fluid.

Fig. 2 shows the equilibrium state between the air liquefaction and cold box. Equations (1) and (2) show the mass balance of the air liquefaction and cold box, respectively. The subscript i in Eqs. (1) and (2) is an index of a substance, $i=1$ shows oxygen, $i=2$ shows nitrogen, and $i=3$ shows other gases. Moreover, Eqs (3) and (4) represent the heat balance of the air liquefaction and cold box, respectively.

$$\dot{m}_s \cdot M_{s,i} = \dot{m}_{cb} \cdot M_{cb,i} \tag{1}$$

$$\dot{m}_{cb} \cdot M_{cb,i} = \dot{m}_l \cdot M_{l,i} + \dot{m}_g \cdot M_{g,i} \tag{2}$$

$$\dot{m}_s \cdot h_s + \dot{Q}_{cb} = \dot{m}_{cb} \cdot h_{cb} \tag{3}$$

$$M_{cb} \cdot C_{cb} \cdot \frac{dT}{dt} = \dot{m}_{l,i} \cdot h_{l,i} - \dot{m}_{g,i} \cdot h_{g,i} - \dot{Q}_{cb,loss} \tag{4}$$

Because liquid air stored in the cold box corresponds to the load change of the IGFC for several minutes or less, the dynamic characteristics of the air compressor is ignored. On the other hand, Eq. (4) represents the dynamic characteristics of the raw material fluid in the cold box.

3.1.2 Transfer function

Equation (5) represents a transfer function for the temperature in the cold box. The dynamic characteristics of the ASU are calculated from Eq. (4), and the transfer function

of Eq. (5) is obtained. The term τ_{cb} in Eq. (5) is the time constant of temperature change in the cold box, which is obtained from Eq. (4). Here, s is a Laplace operator.

$$P_{cb} = \frac{1}{1+\tau_{cb}s} \tag{5}$$

3.2 Coal gasifier

Previous research has reported methods for removing foreign substances such as CO_2 from the product gas [31, 32, 41-42, 44] and for removing acid [45-48]. The reaction of the solid phase of a coal gasifier is the thermolytic reaction of coal and the gasification reaction of char. Because the temperature inside the coal gasifier is very high, a thermolytic reaction occurs instantly. Therefore, the dynamic characteristics of the thermolytic reaction in the coal gasifier can be ignored and the gasification reaction of char and gas phase reaction are investigated.

3.2.1 Mass balance

Table 1 shows reactions accompanying coal gasification. When coal is heated, the thermolytic reaction of coal will occur first. Next, the fuel gas (synthesis gas) is obtained primarily from oxygen, vapor, carbon dioxide, hydrogen, and other gases reacting to the coal char.

Table 1 Fundamental reaction formulas of coal gasification

(1) Thermolytic reaction
$\text{Coal} \rightarrow \text{CH}_4 + \text{C(s)}$

(2) Oxidizing reaction
$C(s) + O_2 \rightarrow CO_2$
(3) Reaction with carbon dioxide
$C(s) + CO_2 \rightarrow 2CO$
(4) Reaction with vapor
$C(s) + H_2O \rightarrow CO + H_2$ $C(s) + 2H_2O \rightarrow CO_2 + 2H_2$ $CO + H_2O \rightarrow CO_2 + H_2$
(5) Reaction with hydrogen
$C(s) + 2H_2 \rightarrow CH_4$, $CO + 3H_2 \rightarrow CH_4 + H_2O$

The speed of the chemical reaction from which substance C is generated from substances A and B under a nonequilibrium state and the multiplier of the concentration C_A and C_B of a substance can be approximated using Arrhenius's equation as a function (Eq. (6)). Moreover, when the reaction of gases A, B, and C are in equilibrium, the reaction speed can be derived using the partial pressure (p_A, p_B) of gases instead of the concentration of substances (Eq. (7)). However, the subscript j of r_j in Eqs. (6) and (7) denotes the number of the target chemical equation, and $A_{i,j}$ is the frequency factor.

$$\frac{dC_C}{dt} = A_{f,j} \cdot \exp\left(-\frac{E_{a,j}}{R \cdot T}\right) \cdot C_A{}^m \cdot C_B{}^n = r_j \cdot C_A{}^m \cdot C_B{}^n \tag{6}$$

$$\frac{dp_C}{dt} = A_{f,j} \cdot \exp\left(-\frac{E_{a,j}}{R \cdot T}\right) \cdot p_A \cdot p_B = r_j \cdot p_A \cdot p_B \tag{7}$$

Reaction numbers 1–3 (j = 1, 2, 3) in Table 2 are the primary reactions of char to the gasifying agents of oxygen, carbon dioxide, and vapor. Numbers 4–8 (j =4, 5, 6, 7, 8) are

the primary gas phase reactions. The terms $r_1 - r_8$ in Table 2 represent the reaction speeds in the Arrhenius's equation shown in Eqs. (6) and (7) [49-52].

The shift equilibrium constant accompanying coal gasification in the coal gasifier can be expressed in the following formula from references [42]. However, $\dot{m}_j$ in the equation is the molar quantity [mol/s] of the gas constituents j, and T_g is temperature of the gas.

$$K_e = \frac{\dot{m}_{CO_2} \cdot \dot{m}_{H_2}}{\dot{m}_{CO} \cdot \dot{m}_{H_2O}} = \exp\left(-3.689 + \frac{4019}{T_g}\right) \tag{8}$$

Table 2 Important chemical reactions [45-49]

Reaction No.	Reaction	Rate [mol/s]	Heat
Thermolytic reaction			
	$\mathrm{Coal}(C_mH_nO_l) \rightarrow CH_4 + C(s)$		
Reactions of char to the gasifying agents			
j = 1	$C(s) + 1/2O_2 \rightarrow CO$	$r_1 = 5.67 \times 10^9 \times e^{(-1.60\times10^5/(RT))}$	–111kJ/mol
2	$C(s) + CO_2 \leftrightarrow 2CO$	$r_2 = 1.6 \times 10^{12} \times e^{(-2.24\times10^4/(RT))}$	172kJ/mol
3	$C(s) + H_2O \rightarrow H_2 + CO$	$r_3 = 1.33 \times 10^3 \times e^{(-1.75\times10^4/(RT))}$	131kJ/mol
Gas phase reactions			
4	$H_2 + 1/2O_2 \rightarrow H_2O$	$r_4 = 1.00 \times 10^{14} \times e^{(-4.20\times10^4/(RT))}$	–242kJ/mol
5	$CO + 1/2O_2 \rightarrow CO_2$	$r_5 = 2.20 \times 10^{12} \times e^{(-1.67\times10^5/(RT))}$	– 283kJ/mol
6	$CH_4 + 1/2O_2 \rightarrow CO + 2H_2$	$r_6 = 3.00 \times 10^8 \times e^{(-1.26\times10^5/(RT))}$	–35.7kJ/mol
7	$CO + H_2O \leftrightarrow CO_2 + H_2$	$r_7 = 2.78 \times 10^3 \times e^{(-1.26\times10^4/(RT))}$	–41.1kJ/mol
8	$CH_4 + H_2O \leftrightarrow CO + 3H_2$	$r_8 = 4.40 \times 10^{11} \times e^{(-1.68\times10^5/(RT))}$	206kJ/mol

The chemical reactions in the coal gasifier shown in Table 2 are the gasification reaction of char and the consecutive gas phase reactions. The chemical reactions and reaction path

shown in Table 2 are expressed using a block diagram organized from the transfer functions shown in Fig. 3. The terms $G_{r1}-G_{r8}$ in Fig. 3 are the transfer functions using the reaction velocities r_1-r_8 shown in Table 2.

3.2.2 Heat Balance

Equation (9) shows the heat balance of the gasification reaction of char and the gas phase reaction. Each item represents the heating value of enthalpy transportation of the substance i; the heating value of the chemical reaction, the amount of heat transfer between the coal particles, fluid, and furnace wall; and heat loss. The term i is a substance output and input in the system. The substances shown in Table 3 are also considered in this study (i = 1, 2, 3, ···, 6). Moreover, $\dot{m}_{cr,j}$ in the equation is the rate [mol/s] of the chemical reaction j shown in Table 2. Furthermore, the convective heat transfer q_c between gas and coal particles (Eq. (10)) and the radiation heat transfer q_r (Eq. (11)) between the furnace wall and fluid are also considered [48]. The Nusselt number in Eq. (10) is calculated by correlation in the Ranz–Marshall equation shown in Eq. (12). The Nusselt number is applied to a turbulent flow.

$$\sum_{i=1}^{N_{cg}}\left(m_i \cdot C_{cg}\right)\frac{dT_{pc}}{dt}=\sum_{i=1}^{N_{cg}}\dot{m}_{cg,in-out,i}\cdot h_{cg,in-out,i}-\sum_{j=1}^{N_{cg,cr}}r_{cg,cr,j}\cdot\dot{m}_{cr,j}-\left(q_C+q_r\right)-q_{loss} \tag{9}$$

$$N_{cg}=6,\ N_{cg,cr}=8$$

Table 3 Notations for components

i	1	2	3	4	5	6
Component	C	O_2	H_2	CO	N_2	H_2O

$$q_c = \pi \cdot d \cdot \lambda_g \cdot Nu \cdot \left(T_{pc} - T_g\right) \tag{10}$$

$$q_r = \sigma \cdot \varepsilon_{wall} \cdot S_{wall} \cdot \left(T_g^4 - T_{wall}^4\right) \tag{11}$$

$$Nu = 2 + 0.6 \cdot Re^{1/2} \cdot Pr^{1/3} \tag{12}$$

3.2.3 Dynamic characteristics

The dynamic characteristics of the coal gasifier are restricted in the later one at the speed of the chemical reaction model or the heat transfer model. Therefore, the analysis of the coal gasifier used a model with a long response time among the consecutive reactions shown in Fig. 3 or the heat balance of Eq. (9).

3.3 SOFC

The model of the dynamic characteristics of the SOFC is based on the author's study report [36].

3.3.1 Mass balance

Equation (13) is a mass balance equation of the anode of the SOFC. In this equation, i is the component of the substance in Table 4, and $n_{ad,rc}$ is the number of chemical reactions of the anode and reformer given in Table 5. Equation (14) is a mass balance equation in the cathode of the SOFC. In this equation, i is the component of the substance shown in Table 4, and $n_{cd,rc}$ is a chemical reaction in the cathode shown in Table 5.

$$\frac{dm_{ad,i}}{dt} = \dot{m}_{ad,in,i} - \dot{m}_{ad,out,i} + \sum_{j=1}^{n_{ad,rc}} a_{ad,ij} r_{ad,j}, \quad i = 1,\ldots,7, \quad n_{ad,rc} = 4 \tag{13}$$

$$\frac{dm_{cd,i}}{dt} = \dot{m}_{cd,in,i} - \dot{m}_{cd,out,i} + \sum_{j=1}^{n_{ad,rc}} a_{cd,ij} r_{cd,j}\ , \quad i = 1,\ldots,7, \quad n_{cd,rc} = 1 \tag{14}$$

The terms $r_{ad,2} - r_{ad,4}$ in Table 5 represent the speed of each chemical reaction. The reaction speed $r_{ad,1}$ of the anode is obtained using Eq. (15). The reaction speeds $r_{ad,2} - r_{ad,4}$ are calculated using Eqs. (16)–(18) [53].

$$r_{ad,1} = r_{cd,1} = \frac{I}{2F} \tag{15}$$

$$r_{ad,2} = \frac{k_2}{p_{ad,H_2}^{2.5}} \left(p_{ad,CH_4} p_{ad,H_2O} - \frac{p_{ad,H_2}^3 p_{ad,CO}}{K_2} \right) \Big/ DEN^2 \tag{16}$$

$$r_{ad,3} = \frac{k_3}{p_{ad,H_2}} \left(p_{ad,CO} p_{ad,H_2O} - \frac{p_{ad,H_2} p_{ad,CO_2}}{K_3} \right) \Big/ DEN^2 \tag{17}$$

$$r_{ad,4} = \frac{k_4}{p_{ad,H_2}^{3.5}} \left(p_{ad,CH_4} p_{ad,H_2O}^2 - \frac{p_{ad,H_2}^4 p_{ad,CO_2}}{K_4} \right) \Big/ DEN^2 \tag{18}$$

Here, DEN in Eqs. (16)–(18) is given by Eq. (19), and $K_{ads,i}$ in Eq. (19) is given by Eq. (20). Moreover, the rate coefficients for reforming reactions k_2, k_3, and k_4 in Eqs. (16)–(18) are calculated using Eq. (21). The equilibrium constants K_2, K_3, and K_4 of the reaction numbers 2–4 in Table 5 are given in Eqs. (22)–(24), respectively. K_2, K_3, and K_4 were used for Eqs. (16)–(18).

$$DEN = 1 + K_{ads,CO} p_{ad,CO} + K_{ads,H_2} p_{ad,H_2} + K_{ads,CH_4} p_{ad,CH_4} + K_{ads,H_2O} p_{ad,H_2O} \Big/ p_{H_2} \tag{19}$$

$$K_{ads,i} = A_{K_{ads,i}} \exp\left(\frac{-\Delta \bar{h}_{ads,i}}{RT} \right), \quad i = H_2,\ CH_4,\ H_2O,\ CO \tag{20}$$

$$k_j = A_{k_j} \exp\left(\frac{-E_j}{RT} \right), \quad j = 2,\ 3,\ 4 \tag{21}$$

$$K_2 = \exp\left(-26830/T + 30.114\right) \tag{22}$$

$$K_3 = \exp\left(4400/T - 4.036\right) \tag{23}$$

$$K_4 = \exp\left(-22430/T + 26.078\right) \tag{24}$$

The rate of molar flow discharged from the anode and cathode is given in Eqs. (25) and (26), respectively, using the choked exhaust flow equation in consideration of the pressure difference at the entrance of each electrode [51]. Moreover, Eq. (27) represents the oxygen utilization factor and fuel (hydrogen) utilization factor of the cathode and anode electrodes.

$$\dot{m}_{ad,out} = \sqrt{k_{ad}\left(p_{ad} - p_{ad,out}\right)} \tag{25}$$

$$\dot{m}_{cd,out} = \sqrt{k_{cd}\left(p_{cd} - p_{cd,out}\right)} \tag{26}$$

$$u_{O_2} = 1 - \frac{\dot{m}_{out,O_2}}{\dot{m}_{in,O_2}}, \quad u_{H_2} = 1 - \frac{\dot{m}_{out,H_2}}{\dot{m}_{in,H_2}} \tag{27}$$

Table 4 Notations for components

i	1	2	3	4	5	6	7
Component	N_2	O_2	H_2	CH_4	H_2O	CO	CO_2

Table 5 Reactions at the reformer and anode and cathode electrodes

Reaction number	Anode reaction	Reaction rate
1	$H_2 + O^{2-} \rightarrow H_2O + 2e^-$	$r_{ad,2}$
2	$CH_4 + H_2O \leftrightarrow CO + 3H_2$	$r_{ad,2}$
3	$CO + H_2O \leftrightarrow CO_2 + H_2$	$r_{ad,3}$
4	$CH_4 + 2H_2O \leftrightarrow CO_2 + 4H_2$	$r_{ad,4}$
Reaction number	Cathode reaction	Reaction rate
1	$0.5O_2 + 2e^- \rightarrow O^{2-}$	$r_{cd,1}$

3.3.2 Energy balance

Equation (28) is the energy balance equation of the SOFC. The temperature change in a sine time of the SOFC balances the sum total of enthalpy change of the anode and cathode, the energetic change of chemical reactions, the DC electric power output (P_{DC}), and the radiation and heat dissipation (q_r , q_{ht}) of heat conduction. Each reaction heat is contained in the term of enthalpy in Eq. (28). The convection and radiation are responsible for major part of stack cooling in the present study and cooling due to excess air is thus minor. Because the study of outlet temperatures as well as temperature profile of the cells are out of scope of this study then such assumption is acceptable. This means that the outlet temperatures would be somewhat lower than expected practically. Of course it affects slightly the power generations of the bottoming cycles (GT and ST) but dynamic responses would not be altered. Note that cell inlet temperature, cell operating temperature and cell outlet temperature are mainly important for cell thermal stresses the and since cell material type and construction are not studied then this issue is irrelevant for the dynamic simulations.

$$C_S \frac{dT}{dt} = \sum_{i=1}^{N} \dot{m}_{ad,in,i} \left(\Delta \bar{h}_{ad,in,i} - \Delta \bar{h}_i \right) + \sum_{i=1}^{N} \dot{m}_{cd,in,i} \left(\Delta \bar{h}_{cd,in,i} - \Delta \bar{h}_i \right) - \sum_{j=1}^{M} \Delta \bar{h}_{rc,j} r_{ad,j} - P_{DC} - q_r - q_{ht} \tag{28}$$

where, $N = 7$, $M = 4$.

3.3.3 Transfer function

The transfer function for the output adjustment of the SOFC is shown in Eq. (29). The term T_{fc} in Eq. (29) is the time constant of the SOFC. Because the output of the SOFC is dependent on cell temperature, T_{fc} is based on the rate of cell temperature change obtained from the energy balance equation (Eq. (28)) for the SOFC.

$$P_{fc,out} = \frac{1}{1 + T_{fc} s} m_{H_2,in} \tag{29}$$

3.4 Gas turbine system

The expression of the relations of G/T to S/T is the same as that for the analysis of dynamic characteristics in the SOFC triple combined cycle [36].

3.4.1 Relational expression for the compressor

The outlet temperature $T_{ac,air,out}$ in the air compressor G/T is calculated using Eq. (30) outdoor air temperature T_{amb}, where the change of air in a compressor assumes adiabatic compression, η_{ac} is compressor efficiency, R_{ac} is the compression ratio of the compressor, $W_{ac,air}$ is the rate of air flow in the compressor, and γ is the ratio of specific heat of air.

$$T_{ac,air,out} = T_{amb} \cdot \left\{ 1 + \frac{\left(R_{ac} \cdot W_{ac,air}\right)^{\frac{\gamma-1}{\gamma}} - 1}{\eta_{ac}} \right\} \tag{30}$$

3.4.2 Gas turbine

Equation (31) represents the inlet temperature $T_{gt,in}$ of the G/T, and Eq. (32) represents the outlet temperature $T_{gt,out}$. Here, the subscript rat expresses the rating assuming that the flow of combustion gas is the same as the rate of air flow rate from the compressor. Furthermore, $\dot{m}_f$ in each equation is the combustion gas flow supplied to the G/T, $\dot{m}_{ac,air}$ is the rate of air flow, and η_{gt} in Eq. (32) is turbine efficiency. Change of the combustion gas in the G/T is assumed to be adiabatic expansion. The dynamic-characteristics analysis and efficiency of the gas turbine are not related.

$$T_{gt,in} = T_{ac,out} + \left(T_{gt,in,rat} - T_{ac,out,rat}\right)\frac{\dot{m}_f}{\dot{m}_{ac,air}} \tag{31}$$

$$T_{gt,out} = \left\{ T_{ac,out} + \left(T_{gt,in,rat} - T_{ac,out,rat}\right) \cdot \frac{\dot{m}_f}{\dot{m}_{ac,air}} \right\} \left\{ 1 - \left(1 - \frac{1}{\left(R_{ac} \cdot \dot{m}_{ac,air}\right)^{\frac{\gamma-1}{\gamma}}} \right) \cdot \eta_{gt} \right\} \tag{32}$$

3.4.3 Transfer function

Equation (33) is a transfer function of the G/T when the time constant τ_{ac} of the compressor is used.

$$P_{gt} = \frac{K_{gt} \cdot \left\{ \left(T_{gt.in} - T_{gt,out}\right) - \left(T_{ac,out} - T_{amb}\right) \right\} \cdot \dot{m}_{ac,air}}{1 + \tau_{ac} s} \tag{33}$$

3.5 Steam Turbine System

3.5.1 Relational expression

It is assumed that the model for the S/T is a Rankine cycle. The external work P_{st} of the S/T is obtained by removing the power consumption P_{pump} of the circulating pump from the heating value P_{boiler} supplied to the exhaust gas boiler, as shown in Eq. (34). Moreover, $\eta_{th,st}$ in the equation is the theoretical thermal efficiency.

$$P_{st} = P_{boiler} \cdot \eta_{th,st} + P_{pump} \tag{34}$$

3.5.2 Transfer function

Because steam supplied from the exhaust gas boiler passes through a steam pipe before working in the turbine, the time lag occurs in the output of the S/T (Steam receiver model). Therefore, the transfer function is given in Eq. (35) by setting the time constant τ_{sr} of the steam receiver. Moreover, the transfer function of the output of S/T is given by Eq. (36) using the delay time constant τ_{boiler} of the exhaust heat recovery boiler, the S/T power coefficient K_{st}, and the steam temperature T_{sm}. Equations (35) and (36) are used in the investigation of the dynamic characteristics of the system. Because the efficiency of the proposed system is not investigated in this study, the fixed value of the efficiency of the steam turbine system does not become a problem.

$$P_{out} = \frac{1}{1+\tau_{sr}s} \cdot P_{in} \tag{35}$$

$$P_{st} = \frac{K_{st} \cdot T_{sm} \cdot \dot{m}_{sm}}{1 + \tau_{boiler} s} \tag{36}$$

4. Modeling of Electric Power Output and the Electric Power Balance Equation

4.1 Electric Power Balance

Equation (37) represents incoming and outgoing electric power in the proposed system during sampling time t. The combined cycle for G/T and S/T is a multiple axes type. The left-hand side of Eq. (37) represents electric power supply, and each item represents the output of the SOFC, G/T generator, and S/T generator. The right-hand side of Eq. (37) expresses the consumption of electricity. In the equation, the DC output of the SOFC is changed into AC through an inverter.

$$P_{fc} + P_{gt} + P_{st} = P_{nd} + P_{loss} \tag{37}$$

4.2 Modeling of Electric Power Output

4.2.1 Whole System

Fig. 4 shows the control block diagram of the proposed IGFC. The quantity of raw material synthesis gas in the ASU is adjusted with the amount of air discharge $\mathrm{CP}_{\mathrm{asu,air}}$ and the amount of coal $\mathrm{PP}_{\mathrm{cgf,coal}}$ supplied by the coal feeder in the gasifier. In addition, the emission temperature of the G/T is adjusted by controlling the rate of air flow $\mathrm{VV}_{\mathrm{cb,air}}$. This ensures a stable supply of heat to the heat recovery steam generator. The bus line in Fig. 4 shows an electric power grid.

4.2.2 Control block

Fig. 5 shows a control block diagram of the proposal IGFC shown in Fig. 4. The fuel gas supplied to the SOFC is adjusted by controlling the supply of fuel derived from exhaust heat temperature and the processing of synthesized gas. To enable a quick response of the SOFC in the fuel supply control system, a proportional-integral-derivative (PID) controller is installed. In addition, because fuel gas is stored in the ASU, load fluctuations of less than a few minutes can be absorbed. Therefore, the time lag of the ASU does not need to be considered. Fig. 6 shows the preferential control of the SOFC output, wherein operation of the G/T and S/T is stopped until the SOFC reaches 50% or more of rated power output.

4.2.3 Electric power system control block

(1) SOFC

Figure 7(a) shows a circuit of the SOFC power system. The DC output of the SOFC is changed into a three phase AC using a snubber circuit, a DC–DC converter, and an inverter. The bus line is supplied through a harmonic filter and an interconnection device. Because the output of the SOFC, G/T, S/T, load, and other power sources are interconnected on the bus line, the frequency of the bus line is changed by the balance of supply and demand. Therefore, the frequency of the bus line is always measured and the inverter is controlled to minimize any deviation in the target frequency. Figure 7(b) shows the control block of the SOFC, where the inverter controls frequency deviation using a PID control device. However, because a time lag occurs in the control described above, the primary delay is taken into consideration using the time constant T_{sofc} .

(2) Gas and Steam Turbines

As shown in Eq. (38), the frequency deviation $\Delta\omega$ of the electric power generated by a rotating machine is based on the difference in supply and demand $(P_s - P_d)$ between the power supply of a rotating machine P_s and power load P_d. Moreover, the magnitude of $\Delta\omega$ depends on the inertia constant M_{fw} of a power source. Equation (39) is a definitional equation for M_{fw}. Slight changes in electric power are eased by proper settings of M_{fw}. Figure 8 shows a block diagram of the frequency control of G/T and S/T on the basis of Eqs. 38 and 39.

$$\Delta\omega = \frac{1}{M_{fw}s} \cdot \frac{1}{\omega} \cdot \left(P_{gt} + P_{st} - P_d\right) \tag{38}$$

$$M_{fw} = J \cdot \omega = \frac{1}{2} a_r^2 \cdot m_r \tag{39}$$

5. Conditions and Method of Analysis

Table 6 shows the rated power and power generation efficiency of each power generator used in the analysis. The total rated power of the system is 100 MW, and the system frequency is 50 Hz.

Table 6 System configurations

System rated power	100 MW
Rated power of SOFC	70 MW
Rated power of G/T	22 MW
Rated power of S/T	8 MW
Power generation efficiency (Rated power, HHV)	
Total	62%

SOFC	43%
G/T	25%
S/T	14%
System frequency	50 Hz

5.1 ASU and Coal Gasifier

Table 7 shows the property values of the coal used in the analysis. Table 8 shows the specifications and operating conditions of the coal gasifier. In addition, the state inside the G/T burner under rated power is set to 3 MPa at 525 K.

Table 7 Physical properties of coal

Australian black coal	
Density	740 kg/m^3
Specific heat	1.3 kJ/(kg･K)
Heat conductivity	0.12 W/(m･K)
Moisture	4.2 wt%
Fixed carbon	56.2 wt%
Volatile matter	30.9 wt%
Ash	8.7 wt%
HHV	30000
C	76.3 wt%
H	5.31 wt%
O	7.31 wt%
N	1.54 wt%
S	0.46 wt%

Table 8 Specifications of the coal gasifier furnace

Furnace	
Diameter and height	4.9 m, 20 m
Height of combustion chamber	4 m
Reaction temperature in furnace	1775 K

Reaction pressure in furnace	6 MPa

5.2 SOFC

Table 9 shows the operating specifications and setting values for the SOFC analysis. Because air–fuel ratio (AFR) influences operating temperature of the SOFC, the range 5–10 is investigated.

Table 9 Equipment specifications and settings

SOFC solid heat capacity	600 J/(kg·K)
SOFC operation pressure	1.0 MPa
SOFC total current	1522 A
SOFC cell voltage	0.657 V
SOFC temperature	1113 K
SOFC stack unit power	99.6 kW
The number of stack unit	740 set
Coal energy input	161.3 MW
Air mass flow rate	992 kg/s
AFR	5, 10, 15
Fuel utilization rate	0.85
Oxygen utilization rate	0.23
Outside air temperature t_{amb}	288 K

5.3 Gas Turbine

Table 10 shows the operating specifications and settings of the air compressor and SOFC.

Table 10 Air compressor and G/T specifications

Compressor outlet temperature $t_{ac,out}$	684 K
G/T entrance temperature $t_{gt,in}$	1573 K
Pressure ratio of compressor R_{ac}	15
Ratio of specific heat γ	1.4

Efficiency of compressor η_{ac}	85%
Turbine efficiency of G/T η_t	85%

5.4 Dynamic Characteristics of Equipment

Table 11 shows the time constant of the transfer function and upper and lower limits of a limiting circuit for the main equipment [54, 55]. The term p.u. in the table is the per unit method based on the rated power.

Table 11 Design parameters and time constants

Equipment	
Delay time constant of compressor T_{ac}	0.2 s
Delay time constant of heat recovery boiler T_b	300 s
Governor-free control of SOFC	
Fuel upper limit $F_{fc,up1}$	1.2 p.u.
Fuel lower limit $F_{fc,lw2}$	0.0 p.u.
Time constant of flow control valve $T_{fc,v}$	4.0 s
Load and speed control of G/T	
Time constant of governor $T_{gt,f}$	0.05 s
Load high limit setting $F_{gt,up1}$	1.1 p.u.
Load low limit setting $F_{gt,lw1}$	0.0 p.u.
Governor-free control of G/T	
Fuel upper limit $F_{gt,up2}$	1.1 p.u.
Fuel flow rate at the time of no load $F_{gt,lw2}$	0.23 p.u.
Time constant of flow control valve $T_{gt,v}$	1.0 s
Fuel system time constant $T_{gt,f}$	0.4 s
Emission temperature control of G/T	
Time constant of radiation shield $T_{gt,rs}$	15 s
Time constant of thermostat $T_{gt,ig}$	2.5 s
Time constant of integral control $T_{gt,t}$	250 s
Control-signal upper limit of temperature of	

exhaust gas $F_{gt,up3}$	1.05
Control-signal lower limit of temperature of exhaust gas $F_{gt,lw3}$	0.0
Reference temperature of exhaust gas of G/T $t_{gt,et0}$	858 K

5.5 Analysis Method

The dynamic characteristics of the proposed IGFC shown in Fig. 1 were analyzed under the fixed step of the relative error 10^{-3} using the MATLAB/Simulink R 2015a. Convergence time was long because the time constant of the ASU and the coal gasifier was large. Therefore, shortening the convergence time was attempted by introducing a PID controller as shown in Fig. 5. The electric power output of the SOFC was the transient overshoot range with a 20% of upper limit, with each parameter of the PID controller set to converge in shortest amount of time. As a result, each parameter was set at the values shown in Table 11.

Table 12 Parameters of the PID controller

K_P	K_I	K_D	F_{cl}
1.979	0.000576	1402	0.04715

6. Results of Analysis

6.1 Step Response Characteristics

6.1.1 Step output

Fig. 9(b) shows the response results for the SOFC, G/T, and S/T at the point when the step load shown in Fig. 9(a) was input to the IGFC. The left side of Fig. 9 shows the response result when the increased step of load was input into the system, and the right

side shows the results when the step of load was decreased. As shown in Fig. 9(a), the input of an increased step and a decreased step at intervals of 30,000 s resulted in step widths of 0.05, 0.1, 0.15, and 0.2 p.u. (5%, 10%, 15%, 20% of the rated load), respectively. The magnitude of the difference in step input shown in Fig. 9(a) and responses shown in Fig. 9(b) appear as the frequency deviation shown in Fig. 9(c). The figure shows that the frequency deviation immediately following a step was large. The frequency deviation became large as the step width increased. However, this tendency was greater with decreased steps than with increased steps. In the case of the largest step width of 0.2 p.u., the convergence time of the step response was approximately 8,000 s.

6.1.2 Speed of chemical reaction and heat transfer

Fig. 10 shows the relation among the AFR, step width, and frequency deviation obtained in Section 6.1.3. Although frequency deviations differed in the increase and decrease steps, there was almost no difference in the frequency deviation of the AFR. The difference in the supply of air in the SOFC compressor was expected to significantly influence the operating temperature of the SOFC. However, as shown in Fig. 10, the reason the response delay of the IGFC was not strongly related to the difference in the AFR was because shortening the convergence time using the PID controller was effective. Although the temperature change resulting from heat transfer in the coal gasifier was 0.253 K/s (Eq. (9)), the speed of each chemical reaction shown in Fig. 3 exceeded the heat transfer speed. Moreover, the dynamic characteristics of the temperature change in the SOFC when AFR = 5, 10, and 15 were 0.0140, 0.0309, and 0.0476 K/s, respectively. On the basis of these

results, to accelerate the IGFC response rate, improvements in the speed of heat transfer and design of redundant equipment in accordance with a transient overshoot are necessary.

6.1.3 Inertia system and frequency deviation

When the inertia constant of the G/T and S/T changed, as shown in Fig. 10, a change a number of frequencies changes was observed. Generally, a minute deviation in frequency decreased when the inertia constant was large. The acceptable range of frequency deviation for the Hokkaido Electric Power Co., Inc. was 50 ± 0.3 Hz. The frequency deviation of the electric power for the G/T and the S/T could not satisfy the conditions outlined in Figs. 9 and 10. These power sources could not respond to the peak supply with a load change.

6.2 Load-Following Characteristics

6.2.1 Pattern of electric power supply

Fig. 11(a) shows the electric power supply pattern of the Hokkaido Electric Power Co., Inc. [56] on a representative day in August 2014. The figure uses the per unit method based on 4.65 GW of maximum output. Electric power was supplied by a combination of thermal and hydraulic power generating facilities in the utility's service area. Some systems of the supplied power corresponded to the output of renewable energy and related large changes in load. Because heat transfer control of the coal gasifier and the SOFC required a long response time, the IGFC was used as a base power source to correspond to uniform load. However, when the IGFC was introduced as the power source or distributed

power supply of a small-scale power network (microgrid), load-following operation to a load change was required. Therefore, the electric power supply pattern shown in Fig. 11(a) was introduced into the IGFC model and the load-following characteristics were analyzed.

6.2.2 Relationship to load fluctuation

Fig. 11(b) shows the response results in two cases, A and B. Although the inertia constant of G/T and S/T in Cases A and B were the same, the AFR differed considerably. The response results in Case A was closer to the load pattern shown in Fig. 11(a) rather than Case B. Moreover, the response characteristics of the SOFC were almost the same as those of the G/T described in Section 6.1. Fig. 11(c) shows the analysis results for the frequency deviation of the G/T. Because the inertia constant of the G/T and S/T were similar set in each case, the frequency deviation of the S/T was the same as that shown in Fig. 11(c). Because the acceptable range of frequency deviation for the Hokkaido Electric Power Co., Inc. was 50 ± 0.3 Hz, the period during which deviation was acceptable was long in each case. Therefore, the electric power output of the SOFC, G/T, and IGFC S/T made it difficult to use them as peak power sources with load fluctuations. Because the response time of the system required to achieve a change of 20% of rated power was approximately 8,000 s, the operational change to the IGFC would have to be initiated 2.2 h in advance.

7. Conclusions

Most investigations of the dynamic characteristics of the IGFC are not readily available and the load-following characteristics of interconnections with renewable energy or a load with fluctuations is not well known. In this study, the analytic model of the IGFC was developed and the dynamic characteristics of the model were investigated using the MATLAB/Simulink R 2015a. Because of the difference in electric power supply and demand appeared as a frequency deviation in the power network, the magnitude of the frequency deviation was used for evaluating the dynamic characteristics of the IGFC. Moreover, the analysis model of the IGFC was 100 MW of full force power. The rated power of the SOFC, G/T, and S/T was 70 MW, 22 MW, and 8 MW, respectively. Consequently, the following conclusions were obtained.

(1) The step response characteristics and dynamic characteristics of the IGFC using a power load pattern (Hokkaido Electric Power Co., Inc. during the summer season in Japan) were clarified. In the numerical analysis, the dynamic characteristics of the IGFC were clarified with respect to the inertia constant of each turbine and the AFR of the SOFC.

(2) When the magnitude of an input step (step width) increased, the frequency deviation of the electric power resulting from the step response of the IGFC became large. This tendency was larger in the decrease step pattern than in the increase step pattern. The convergence time of the step response was about 8,000 s to achieve a 20% increase in rated power. Because the speed of chemical reactions of the coal gasifier and SOFC were faster than the heat transfer speed, a high speed heat transfer control was necessary to improve the response speed of the IGFC. Furthermore, to shorten the convergence time, a redundancy design of equipment is necessary.

(3) The acceptable range of the frequency deviation of the Hokkaido Electric Power Co., Inc. was 50 ± 0.3 Hz. When the dynamic characteristics of the IGFC were investigated in relation to the power load pattern of the Hokkaido Electric Power Co., Inc., the real time response to the load pattern was difficult for the SOFC. For the G/T and S/T, the frequency deviation of electric power output deviated from the acceptable range during the representative day. When the 20% of load change in rated power was applied to the IGFC, achieving the stability of the output required approximately 2.2 h. Therefore, adjustments to the output of the IGFC need to be planned several hours in advance.

Nomenclature

ASU	:	Air separation unit
A_i	:	Pre-exponential factor for i
a	:	Stoichiometric matrix
a_r	:	Flywheel plate radius [m]
C_p	:	Specific heat at constant pressure [J/K]
$CP_{asu,air}$	:	Air compressor of ASU
$CP_{asu,air1}$	:	Compression turbine of ASU
C	:	Heat capacity [J/(K･kg)]
C_A, C_B	:	Concentration
DEN	:	Denominator
d	:	Characteristic length [m]
E	:	Activity energy [J/mol]

E_{ocv}	:	Open circuit voltage [V]
$\mathrm{ET}_{\mathrm{asu,air}}$	:	ASU expansion turbine
F	:	Faraday constant (96,485 sA/mol)
F_{cl}	:	PID control filter factor
G	:	Transfer function
G/T	:	Gas turbine
h	:	Enthalpy [J/g]
$\Delta\bar{h}$	:	Molar specific enthalpy [J/mol]
I	:	Current [A]
J	:	Moment of inertia [kgm^2]
K	:	Equilibrium constant
K_{ads}	:	Adsorption constant
K_D, K_I, K_P	:	PID control parameter
K_h	:	Coefficient of overall heat transfer [W/(m^{2}K)]
K_{st}	:	Power coefficient of S/T
k	:	Rate coefficients for reforming reactions
M	:	Mass [g]
M_{fw}	:	Factor of inertia
m	:	Number of moles [mol]
$\dot{m}$	:	Moles rate [mol/s], Mass rate [g/s]
m_r	:	Mass of flywheel plate [kg]
N	:	Number

$n_{ad,rc}$	:	Number of chemical reactions in anode
$n_{cd,rc}$	:	Number of chemical reactions in cathode
Nu	:	Nusselt number
P	:	Power [W], [p.u.]
P_d	:	Power load [W], [p.u.]
P_s	:	Power supply [W], [p.u.]
p	:	Pressure [Pa]
pc	:	Pulverized coal
$\mathrm{PP}_{\mathrm{cgf,coal}}$	:	Supply of coal by feeder [g/s]
Pr	:	Prandtl number
$\dot{Q}$	:	Heat [W]
q_C	:	Convective heat transfer [W]
q_r	:	Radiative heat transfer [W]
q_{ht}	:	Heat conduction [W]
R	:	Universal gas constant [J/(mol K)]
r	:	Reaction rate [mol/s]
R_{ac}	:	Air compressor compression ratio
Re	:	Reynolds number
S	:	Area [m^2]
s	:	Laplace operator
(s)	:	Solid
SOFC	:	Solid oxide fuel cell

S/T	:	Steam turbine
T	:	Temperature [K]
ΔT	:	Temperature difference [K]
T_{amb}	:	Outside air temperature [K]
t	:	Time [s]
u	:	Utilization
V	:	Voltage [V]
$VV_{cb,air}$	:	Combustor air flow valve
W	:	Quantity of flow [p.u.]

Greek characters

ε	:	Emissivity
γ	:	Ratio of specific heat
η	:	Efficiency
η_{th}	:	Theoretical thermal efficiency
λ	:	Thermal conductivity [W/(mk)]
σ	:	Stefan–Boltzmann constant 5.67×10^{-8} [W/(m^2 K^4)]
τ	:	Time constant
ω	:	Frequency
$\Delta\omega$	:	Frequency deviation [Hz]
γ	:	Ratio of specific heat

Subscript

ac	:	Air compressor

ad	:	Anode
amb	:	Ambiance
cb	:	Cold box
cd	:	Cathode
cg	:	Coal gasifier
cr	:	Chemical reaction
DC	:	Direct current
fc	:	Fuel cell
g	:	Gas
gt	:	Gas turbine
hex	:	Heat exchanger
l	:	Liquid
nd	:	Need
pc	:	Pulverized coal
rat	:	Rating
s	:	Supply air
sm	:	Steam
st	:	Steam turbine

References

[1] Siefert S N, Litster S. Exergy and economic analyses of advanced IGCC–CCS and IGFC–CCS power plants. 2013;107:315–328.

[2] Herdem M S, Farhad S, Dincer I, Hamdullahpur F. Thermodynamic modeling and assessment of a combined coal gasification and alkaline water electrolysis system for hydrogen production. Int J Hydrogen Energy 2014;39:3061–3071.

[3] Nagel F P, Schildhauer T J, McCaughey N, Biollaz S M A. Biomass-integrated gasification fuel cell systems – Part 2: Economic analysis. Int J Hydrogen Energy 2009;34:6826–6844.

[4] Doherty W, Reynolds A, Kennedy D. Process simulation of biomass gasification integrated with a solid oxide fuel cell stack. Journal of Power Sources 2015;277:292–303.

[5] Li M, Rao A D, Brouwer J, Samuelsen G S. Design of highly efficient coal-based integrated gasification fuel cell power plants. Journal of Power Sources 2010;195:5707–5718.

[6] Li M, Brouwer J, Rao A D, Samuelsen G S. Application of a detailed dimensional solid oxide fuel cell model in integrated gasification fuel cell system design and analysis. Journal of Power Sources 2011;196:5903–5912.

[7] Bellomare F, Rokni M. Integration of a municipal solid waste gasification plant with solid oxide fuel cell and gas turbine. Renewable Energy 2013;55:490–500.

[8] Wang Y, Yu J, Weng S. Numerical investigation of different loads effect on the performance of planar electrode supported SOFC with syngas as fuel. In J Hydrogen Energy 2011;36:5624–5631.

[9] Obara S, Morel J. Microgrid composed of three or more SOFC combined cycles without accumulation of electricity. Int J Hydrogen Energy 2014;39:2297–2312.

[10] Mehrpooya M, Akbarpour S, Vatani A, Rosen M A. Modeling and optimum design of hybrid solid oxide fuel cell-gas turbine power plants. Int J Hydrogen Energy 2014;39:21196–21214.

[11] Chen S, Lior N, Xiang W. Coal gasification integration with solid oxide fuel cell and chemical looping combustion for high-efficiency power generation with inherent CO_2 capture. Applied Energy 2015;146:298–312.

[12] Grol E. Technical Assessment of an Integrated Gasification Fuel Cell Combined Cycle with Carbon Capture. Energy Procedia 2009;1:4307–4313.

[13] Tsukada M, Abe K, Yonemochi Y, Ameyama A, Kamiya H, Kambara S, Moritomi H, Uehara T. Dry gas cleaning in coal gasification systems for fuel cells using composite sorbents. Powder Technology 2008;180:232–238.

[14] Sardesai P, Seames W, Dronen L, Kozliak E. Exploring the gas-phase anaerobic bioremoval of H_2S for coal gasification fuel cell feed streams. Fuel Processing Technology 2006;87:319–324.

[15] Trembly J P, Gemmena R S, Bayless D J. The effect of IGFC warm gas cleanup system conditions on the gas–solid partitioning and form of trace species in coal syngas and their interactions with SOFC anodes. Journal of Power Sources 2007;163:986–996.

[16] Lanzinia A, Kreutzb T G, Martellic E, Santarelli M. Energy and economic performance of novel integrated gasifier fuelcell (IGFC) cycles with carbon capture. International Journal of Greenhouse Gas Control 2014;26:169–184.

[17] Siefert N S. Chang B Y, Litster S. Exergy and economic analysis of a CaO-looping gasifier for IGFC–CCS and IGCC–CCS. Applied Energy 2014;128:230–245.

[18] Parker P, Shell coal gasification process update, in: GTC Conference: Economics, Performance and Reliability. Gasification Technologies Council, 2006.

[19] Kosuge K, Namiki Y, Itonaga M, Kozuru H, Takeda S, Development of ECOPRO Coal Gasification process ~Results of pilot plant operation and future development towards demonstration plant~. Nippon Steel & Sumitomo Metal Technical Report 2011;2:2–9.

[20] Park S, Ye I, Oh J, Ryu C, Koo J H. Gas and particle flow characteristics in the gas reversing chamber of a syngas cooler for a 300 MWe IGCC. Applied Thermal Engineering 2014;70:388-396.

[21] Naraharisetti P K, Lakshminarayanan S, Karimi I A. Design of biomass and natural gas based IGFC using multi-objective optimization. Energy 2014;73:635–652.

[22] El-Emam R S, Dincer I. Thermal modeling and efficiency assessment of an integrated biomass gasification and solid oxide fuel cell system. International Journal of Hydrogen Energy 2015;1–13.

[23] Rokni M. Biomass gasification integrated with a solid oxide fuel cell and Stirling engine. Energy 2014;77:6–18.

[24] Nagel F P, Ghosh S, Pitta C, Schildhauer T J, Biollaz S. Biomass integrated gasification fuel cell systems–Concept development and experimental results. Biomass and Bioenergy 2011;35:354–362.

[25] Nagel F P, Schildhauer T J, McCaughey N, Biomass-integrated gasification fuel cell systems – Part 1: Definition of systems and technical analysis. International Journal of Hydrogen Energy 2009;34:6809–6825.

[26] Nagel F P, Schildhauer T J, McCaughey N, Biollaz S M A. Biomass-integrated gasification fuel cell systems – Part 2: Economic analysis. International Journal of Hydrogen Energy 2009;34:6826–6844.

[27] Naraharisetti P K, Lakshminarayanan S, Karimi I A. Design of biomass and natural gas based IGFC using multi-objective optimization. Energy 2014;73:635–652.

[28] Pierobon L, Rokni M, Larsen U, Haglind F. Thermodynamic analysis of an integrated gasification solid oxide fuel cell plant combined with an organic Rankine cycle. Renewable Energy 2013;60:226–234.

[29] Rokni M. Thermodynamic analyses of municipal solid waste gasification plant integrated with solid oxide fuel cell and Stirling hybrid system. International Journal of Hydrogen Energy 2014;1–15.

[30] Rokni M. Thermodynamic and thermoeconomic analysis of a system with biomass gasification, solid oxide fuel cell (SOFC) and Stirling engine. Energy 2014;76:19–31.

[31] Gazzani M, Manzolini G, Macchi E, Ghoniemb AF. Reduced order modeling of the Shell-Prenflo entrained flow gasifier. Fuel 2013;14:822–37.

[32] Yang Z, Wang Z, Wu Y, Li Z, Ni W. Use of a reactor network model in the design and operation of a new type of membrane wall entrained flow gasifier. Energy Fuels 2013;27:6322–6332.

[33] Tygue S. Doyle, Zahir Dehouche, Sinisa Stankovic. Decentralized power and heat derived from an eco-innovative integrated gasification fuel cell combined cycle fuelled by waste. International Journal of Hydrogen Energy 2015;40:9013-9025.

[34] Galeno G, Minutillo M, Perna A. From waste to electricity through integrated plasma gasification/fuel cell (IPGFC) system. International Journal of Hydrogen Energy 2011;36:1692-1701.

[35] Sahraei M H, McCalden D, Hughes R, Ricardez-Sandoval L A, A survey on current advanced IGCC power plant technologies, sensors and control systems. Fuel 2014;137:245–259.

[36] Obara S. Dynamic-characteristics Analysis of an Independent Microgrid Consisting of a SOFC Triple Combined Cycle Power Generation System and Large-scale Photovoltaics. Applied Energy 2014;141:19–31.

[37] Rokni M. Introduction of a fuel cell into a combined cycle: a competitive choice for future cogeneration. ASME COGEN-TURBO POWER 93, 7th Congress & Exposition on Gas Turbines In Cogeneration and Utility Industrial and Independent power Generation, (Eds. H. W. Holland, W. E. Hauhe JR., D. H. Cooke, and H. Lukas), ASME 1993: IGTI-Vol. 8: 255–262.

[38] Mitsubishi to develop SOFC-turbine triple combined cycle system. Fuel Cells Bulletin 2012;7:5–6.

[39] Seliger B, Hanke-Rauschenbach R, Hannemann F, Sundmacher K. Modelling and dynamics of an air separation rectification column as part of an IGCC power plant. Sep Purif Technol 2006;49:136–48.

[40] Guo Y, Lu J. Control-oriented dynamic modeling of the air separation unit column in IGCC. IEEE 2011:2600–3.

[41] Adams II TA, Barton PI. A dynamic two-dimensional heterogeneous model for water gas shift reactors. International Journal Hydrogen Energy 2009;34:8877–91.

[42] Sun B, Liu Y, Chen X, Zhou Q, Su M. Dynamic modeling and simulation of shell gasifier in IGCC. Fuel Process Technol 2011;92:1418–1425.

[43] Li C, Dai Z, Sun Z, Wang F. Modeling of an opposed multiburner gasifier with a reduced-order model. Ind Eng Chem Res 2013;52:5825–5834.

[44] Monaghan RFD, Ghoniem AF. Simulation of a commercial-scale entrained flow gasifier using a dynamic reduced order model. Energy Fuels 2012;26:1089–1106.

[45] Jillson KR, Chapalamadugu V, Ydstie BE. Inventory and flow control of the IGCC process with CO_2 recycles. J Process Control 2009;19:1470–1485.

[46] Harun N, Nittaya T, Douglas P, Croiset E, Ricardez-Sandoval LA. Dynamic simulation of MEA absorption process for CO_2 capture from power plants. Int J Greenh Gas Control 2012;10:295–309.

[47] Bhattacharyya D, Paul P, Turton R, Zitney SE. Constrained Nonlinear State Estimation of An Acid Gas Removal Process As Part of An Integrated Gasification Combined Cycle (IGCC) Power Plant with CO_2 Capture. Annual Meeting, Computing and Systems Technology Division, (Eds. Daoutidis, P. and Christofides, P. D.), AIChE 2011:622.

[48] Bhattacharyya D, Turton R, Zitney SE. Transient studies of an integrated gasification combined cycle (IGCC) plant with CO_2 capture. AIChE Annual Meeting. Salt lake city, Utah; 2010.

[49] Lee J C, Lee H H, Joo Y J, Lee C H, Oh M. Process simulation and thermodynamic analysis of an IGCC (integrated gasification combined cycle) plant with an entrained coal gasifier. Energy 2014;64:58–68.

[50] Blasi CD. Dynamic behaviour of stratified downdraft gasifiers. Chem Eng Sci 2000;55(15):2931–2944.

[51] Westbrook CK, Dryer FL. Simplified reaction mechanisms for the oxidation of hydrocarbon fuels in flames. Combust Sci Technol 1981;27(1e2):31–43.

[52] Watanabe H, Otaka M. Numerical simulation of coal gasification in entrained flow coal gasifier. Fuel 2006;85(12e13):1935–1943.

[53] Kandepu R, Imsland L, Foss BA, Stiller C, Thorud B, Bolland O. Modeling and control of a SOFC-GT-based autonomous power system. Energy 2007;32-4:406-417.

[54] Task Force C 4-02-25: Modeling of gas turbines and steam turbines in combined cycle power plant, CIGRE Technical Brochure 2003.

[55] Baba K, Kakimoto N, Dynamic Behavior of Combined Cycle Power Plant for Frequency Drop. IEEJ Transactions on Power and Energy 2002;122:392–400. In Japanese.

[56] Electricity status-of-use data in 2010, The past electricity status-of-use data, Hokkaido Electric Power Co., Inc., http://denkiyoho.hepco.co.jp/download.html ;2014

Caption

Fig. 1 Proposed IGFC combined cycle

Fig. 2 General schematic of the air separation unit equilibrium stage

Fig. 3 Transfer function block of the coal gasification chemical reaction

Fig. 4 Whole system diagram of proposed system

Fig. 5 Control block diagram of proposed system

Fig. 6 Control flow of each generator

Fig. 7 Control block diagram of the SOFC

Fig. 8 Frequency control of electric power output

Fig. 9 Results of step input analysis (M_{gt} = 15, M_{st} = 15, AFR = 15)

(a) Input load

(b) Output power

(c) Frequency variation

Fig. 10 Results of the frequency deviation analysis

Fig. 11 Dynamic characteristics of the proposed system

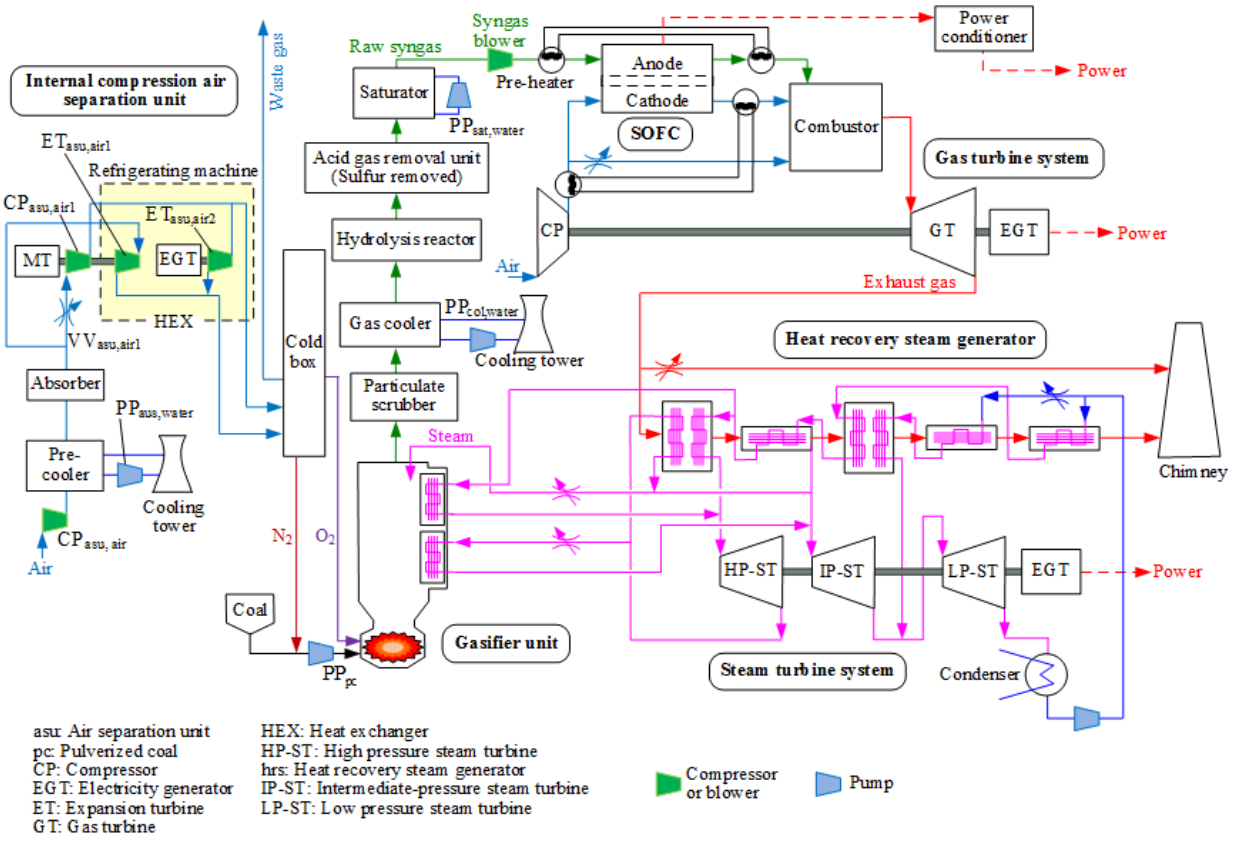

Fig. 1 Proposed IGFC combined cycle

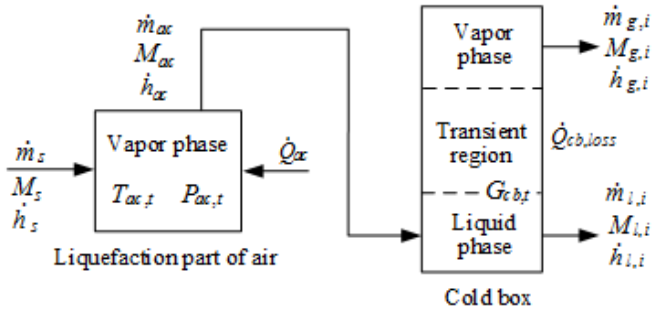

Fig. 2 General schematic of the air separation unit equilibrium stage

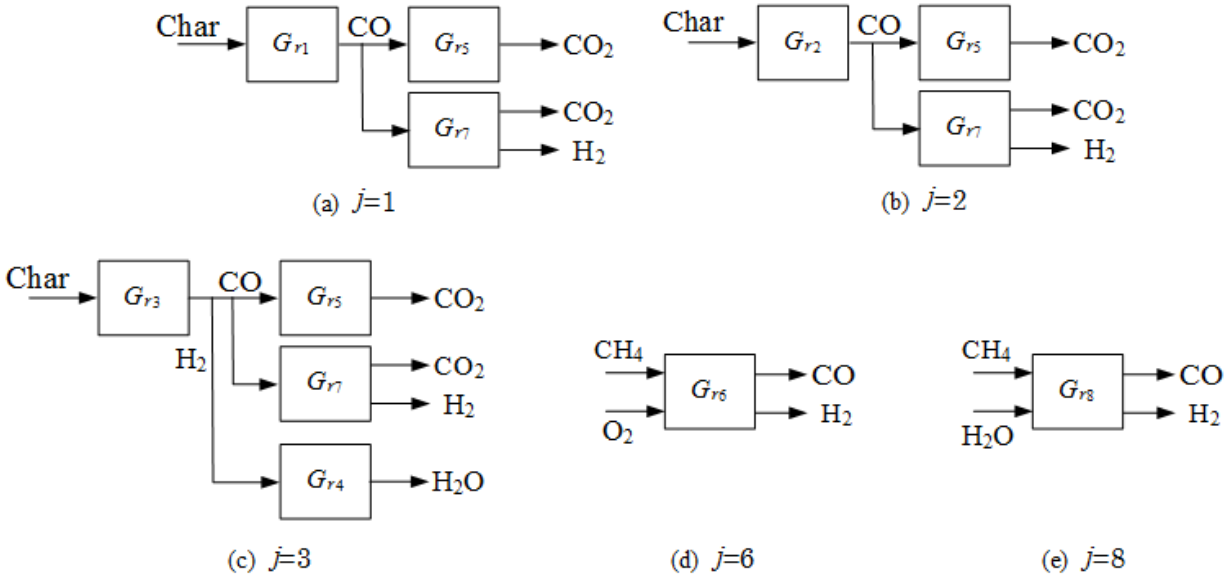

Fig. 3 Transfer function block of the coal gasification chemical reaction

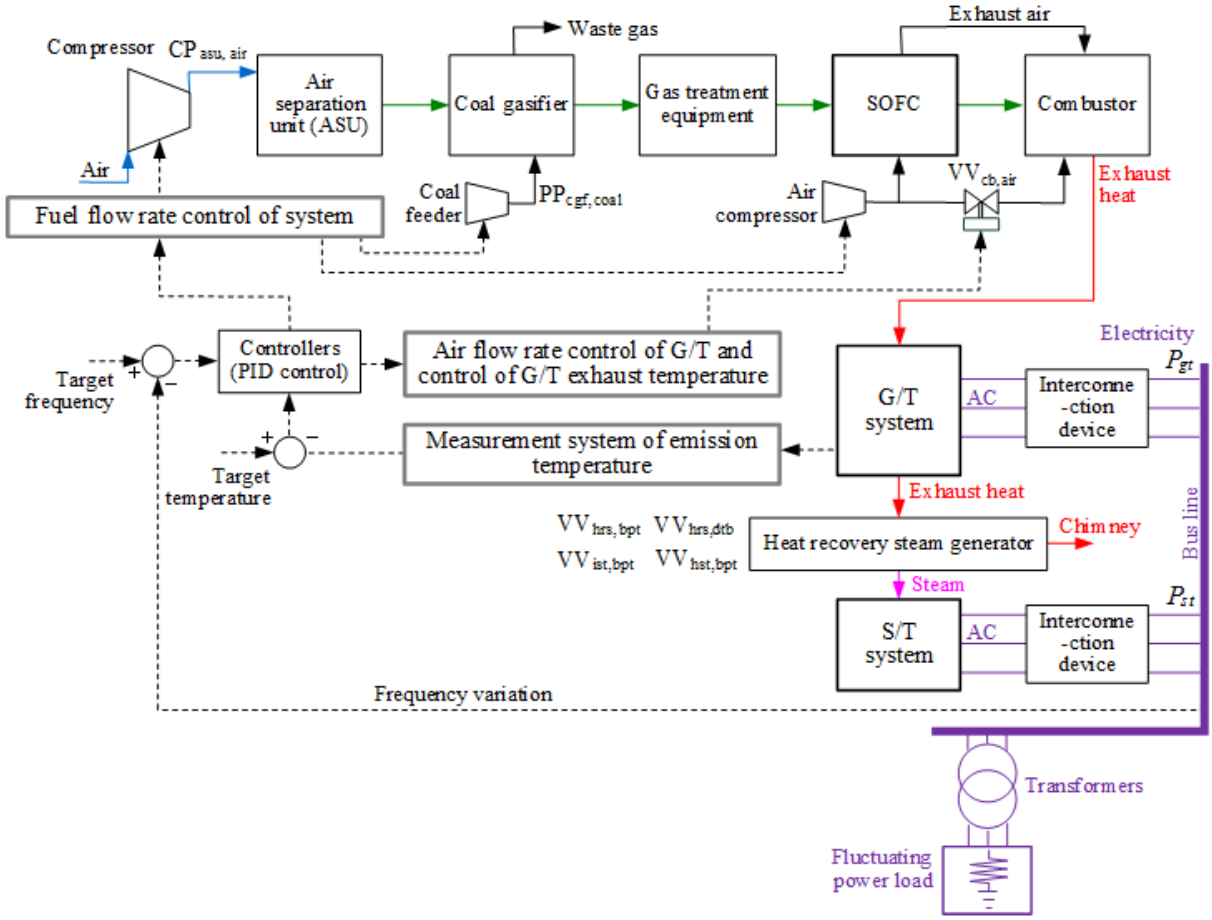

Fig. 4 Whole system diagram of proposed system

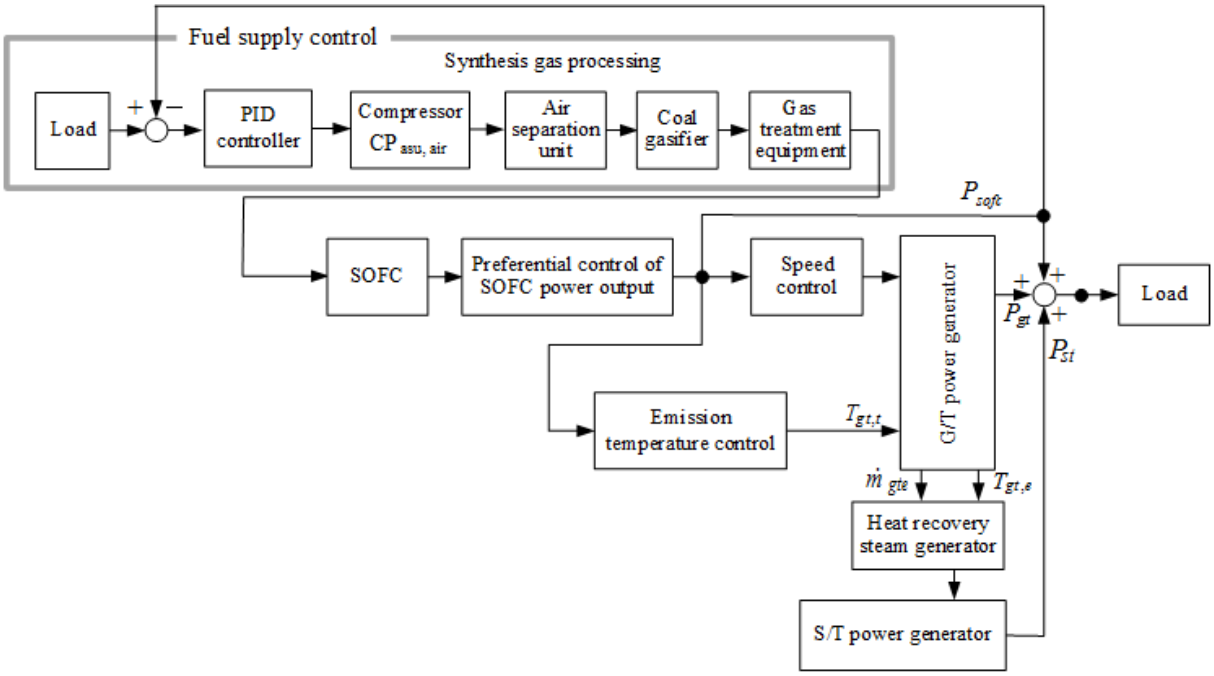

Fig. 5 Control block diagram of proposed system

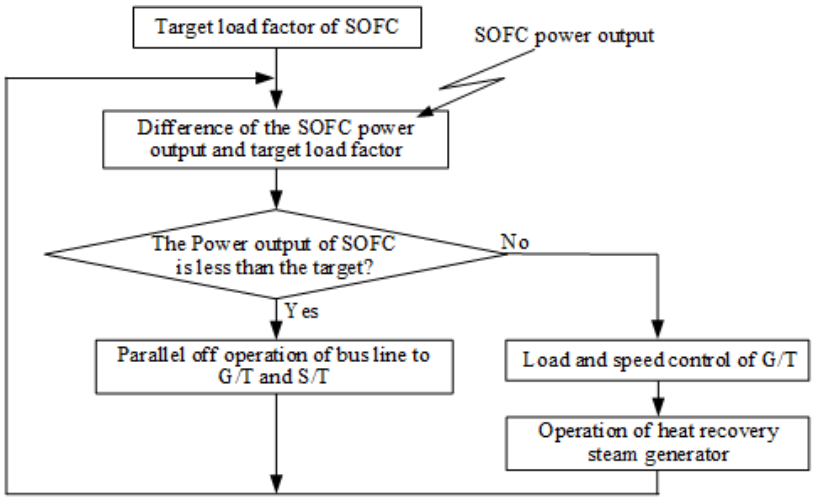

Fig. 6 Control flow of each generator

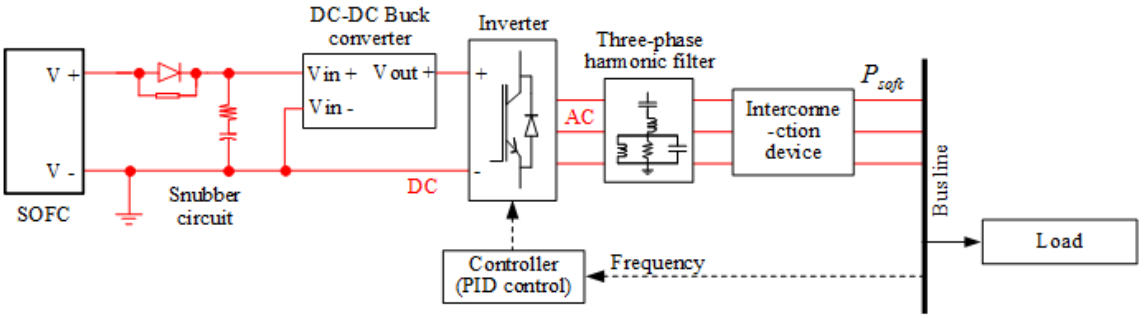

(a) Power circuit

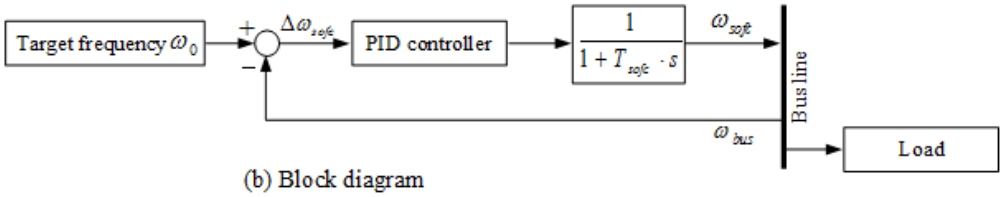

(b) Block diagram

Fig. 7 Control block diagram of the SOFC

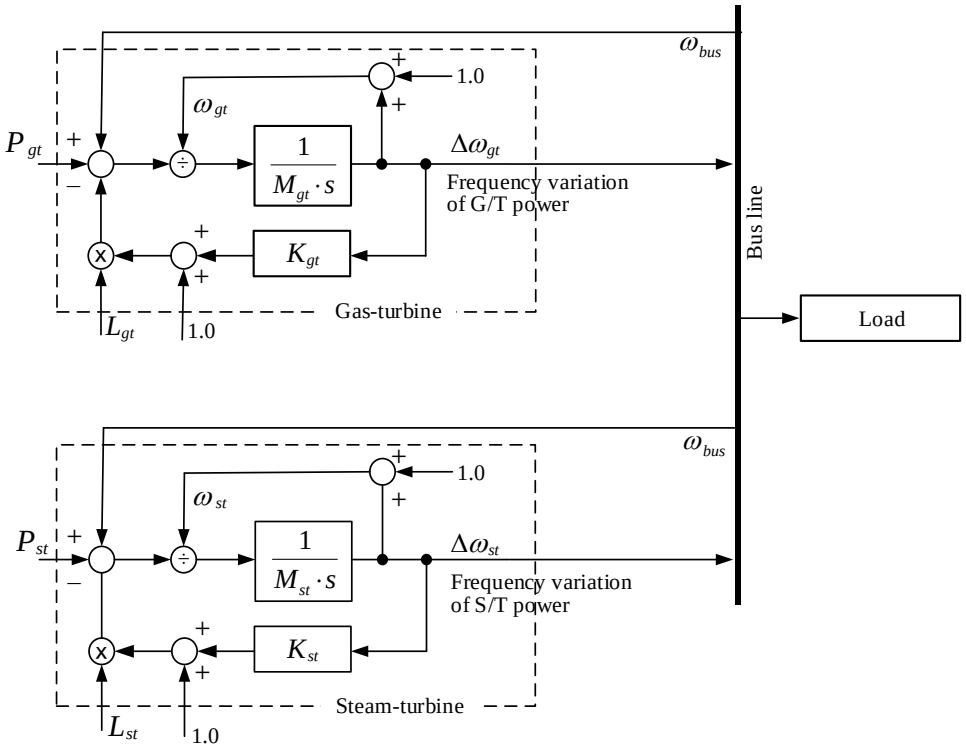

Fig. 8 Frequency control of electric power output

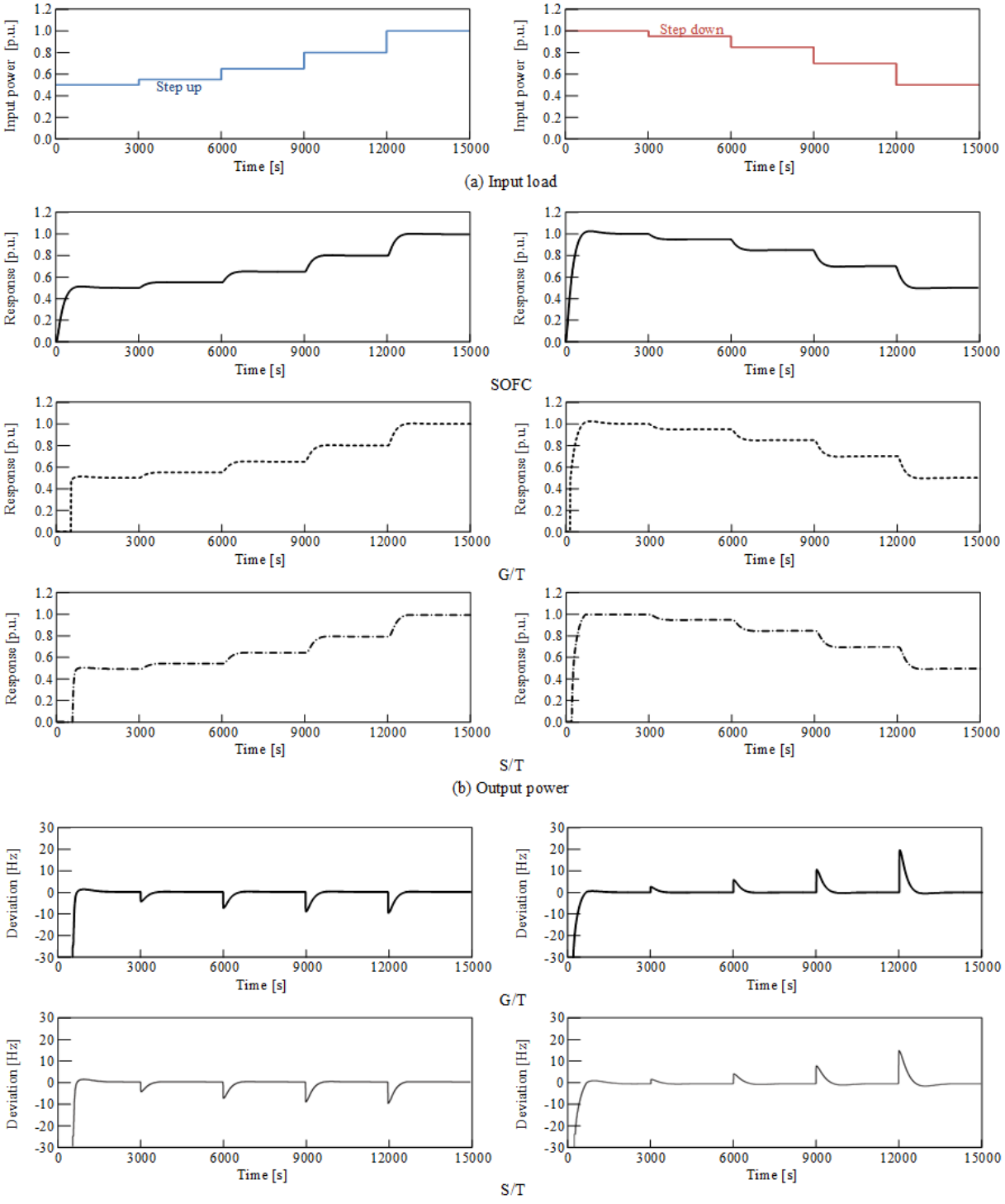

Fig. 9 Results of step input analysis ($M_{gt} = 15$, $M_{st} = 15$, $AFR = 15$)

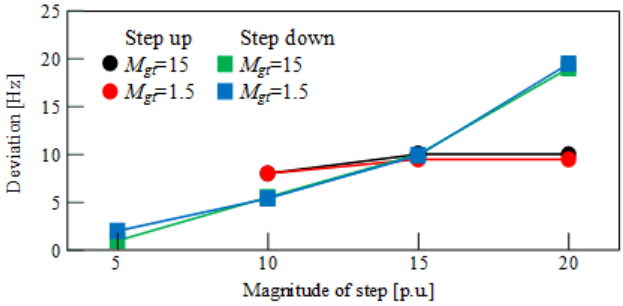

(a) AFR=5

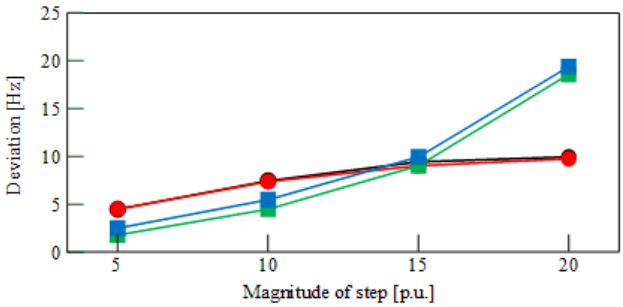

(b) AFR=10

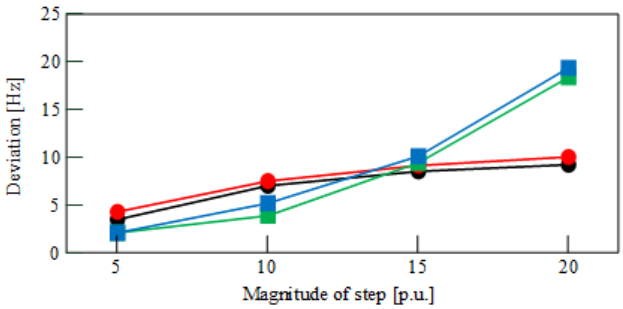

(c) AFR=15

Fig. 10 Results of the frequency deviation analysis

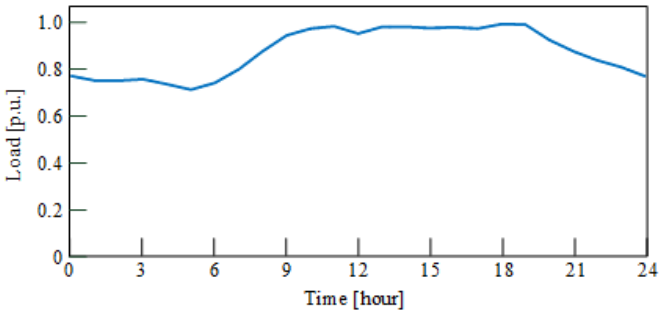

(a) Load pattern

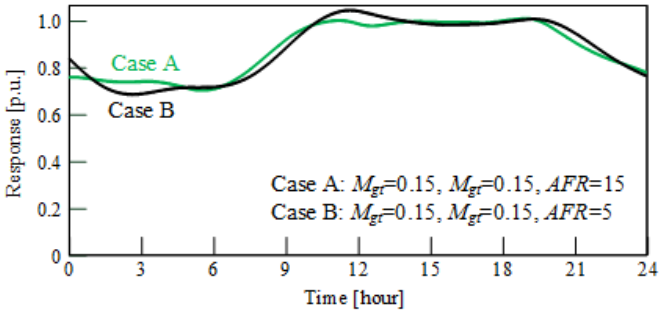

(b) Output of G/T and S/T

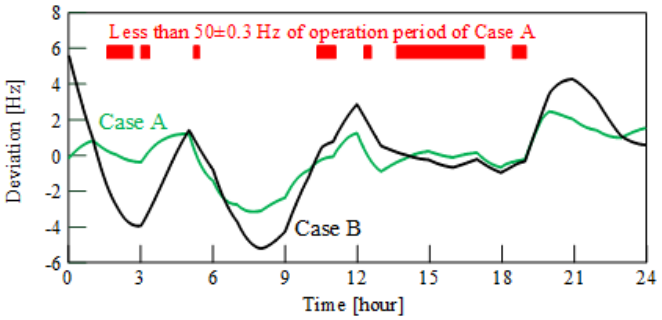

(c) Frequency deviation of output power by G/T and S/T

Fig. 11 Dynamic characteristics of the proposed system